Analysis of Thermal Radiation from an Inhomogeneous Cylindrical Human Body Model

NIKOLAOS K. UZUNOGLU, MEMBER, IEEE, P. G. COTTIS, AND PETROS S. PAPAKONSTANTINOU

Abstract—**The thermal radiation from a cylindrical human body model at microwave frequencies is treated analytically. The human body model is taken to be a homogeneous cylinder at temperature T having a localized internal thermal inhomogeneity at temperature $T + \Delta T$. The mean energy density for the near field outside the cylinder is determined by employing the dyadic Green's function of the homogeneous cylinder and the fluctuation-dissipation theorem. Analytical results are derived for the contributions of the homogeneous cylinder and the inhomogeneity region. Numerical results are presented for several geometries at low microwave frequencies where a reasonable transparency of tissues is expected. The possibility of using microwave radiometry techniques to measure temperature distributions in depth is discussed in relation to hyperthermia and the development of noninvasive diagnostic techniques. It is shown that the emission from surrounding tissues limits the detectability of thermal inhomogeneities inside the body and that by using low microwave frequencies (~ 1 GHz), temperature measurement at depths up to 2 cm can be performed.**

I. Introduction

THE POSSIBILITY of employing passive microwave radiometry techniques to measure temperature distributions deep inside biological systems has recently been suggested by several researchers [1]–[5]. Several experimental radiometry systems have been constructed and tested [5]–[7].

The increasing use of hyperthermia techniques in the treatment of cancer, where accurate temperature measurements are needed, and the inability of infrared radiometers to provide in-depth temperature profiles for diagnostic purposes call for the search of new noninvasive thermometry techniques. In addition to microwave thermography, several other noninvasive techniques have been proposed, such as microwave tomography [8], ultrasonic tomography, nuclear magnetic resonance, and computer tomography [9].

In this paper, temperature measurement based on microwave radiometry is investigated by employing analytical techniques. A full electromagnetic wave analysis is pursued to treat the thermal microwave emission from a cylindrical human body model with an internal inhomogeneity. The low-frequency microwave spectrum is thought to be suitable, since at 0.5–3 GHz frequencies reasonable transparency of tissues can be achieved, while reasonable resolution can be obtained with antennas of manageable size. Up to now the theory of radiative transfer has been employed to estimate the performance of proposed radiometry systems [10].

According to thermodynamic principles, absorption of electromagnetic energy by a material medium is the transformation of radiation into thermal energy, which is accompanied by a rise in the thermometric temperature of the material. The reverse process, that of thermal emission, serves to create the balance between absorbed external radiation and radiation emitted by the material surface. A common example is the absorption of solar radiation from the earth's surface and the thermal radiation from the earth's surface. These transformation processes have been treated in the past by applying the theory of radiative transfer for infrared and visible electromagnetic waves [11]. Recently, corrections to the classical radiative transfer theory have been introduced when analyzing the performance of passive microwave remote sensing systems [12].

The radiative transfer theory makes extensive use of the basic ideas of geometrical optics. In remote sensing systems, this assumption is valid, since the observed media are in the far field and only average properties of the emitting surfaces need to be known. For the problem addressed in this paper, the observed medium and its internal inhomogeneity dimensions are of the order of the detected radiation wavelength. Furthermore, nearfield measurements are performed concerning the thermal radiation. Therefore, the classical radiative transfer theory can only be used approximately to estimate either the resolution or the penetration depth of microwave radiometers in noninvasive thermometry systems.

Based on the fluctuation theory, Rytov [13] considered the case of an infinite isotropic medium. The emission from a homogeneous isothermal sphere has been treated by Kattawar and Eisner [14].

In Fig. 1, the geometry of the cylindrical human body model is given. The cylindrical body is taken to be of infinite length and its radius is designated by α. The frequency-dependent electromagnetic properties of the body are assumed to be known and are defined in terms of the relative dielectric permittivity ϵ_r and the conductivity σ (S/m) [15]. Therefore, the human body is taken to be

Manuscript received January 8, 1987; revised April 10, 1987.

The authors are with the Department of Electrical Engineering, National Technical University of Athens, Athens 10682, Greece.

IEEE Log Number 8715412.

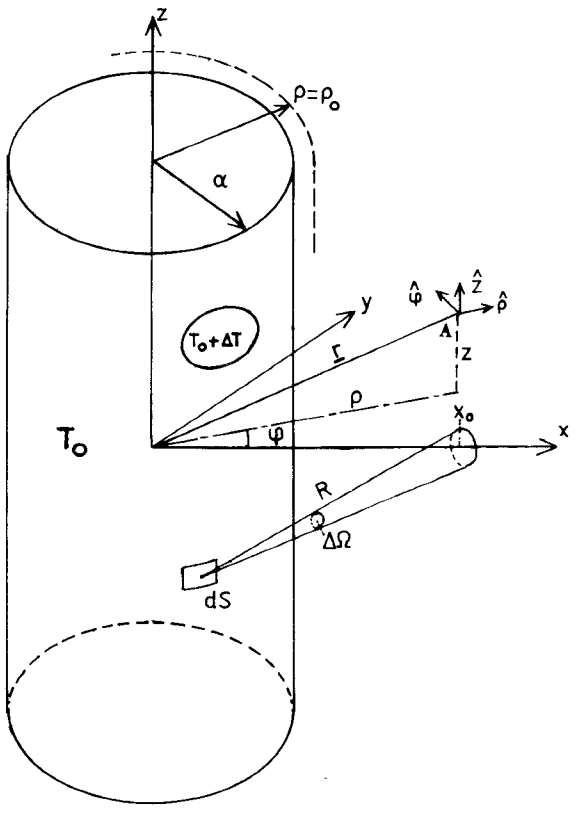

Fig. 1.

electromagnetically homogeneous. Extension to three-layer cylindrical bodies can be easily performed by modifying the present analysis. The values of ϵ_r and σ are taken equal to those of high-water-content tissues (muscle), since the human body consists mainly of tissues of this type. The whole space is magnetically homogeneous and the magnetic permeability is equal to that of free space $\mu_0 = 4\pi \cdot 10^{-7}$ (H/m). The cylinder is surrounded by air with a dielectric permittivity $\epsilon_0 = 10^{-9}/(36\pi)$ (F/m).

A uniform temperature distribution $T = T_0$ is assumed throughout the human body model, except that inside the body a localized inhomogeneity of finite volume V_i at temperature $T_0 + \Delta T$ is considered, as shown in Fig. 1. In the following section, the average thermal energy density is computed at an external point A (see Fig. 1). The Green's functions theory for the infinite cylinder is utilized to take into account the boundary conditions on the cylinder surface. An analytical relation is derived for the radiation energy density, which requires extensive numerical integrations to produce numerical results. The computed results are compared with those obtained by applying the classical radiative transfer theory. Finally, the resolution capability of microwave radiometers is also discussed.

In the following analysis, the field quantities are assumed to have an $\exp(-j\omega t)$ time dependence.

II. Mathematical Formulation of the Problem

The tissues, being linear conductive media, support fluctuating currents creating thermal radiation. The corresponding weak current densities $\boldsymbol{J}(\boldsymbol{r})$ (A/m^2) can only be described statistically by means of the dyadic correlation function [12]

$$\langle \boldsymbol{J}(\boldsymbol{r})\boldsymbol{J}^*(\boldsymbol{r}')\rangle = \frac{4k_B T(\boldsymbol{r})\sigma(\boldsymbol{r})}{\pi}\Delta\omega\,\delta(\boldsymbol{r}-\boldsymbol{r}')\bar{\boldsymbol{I}} \quad (1)$$

where $\bar{\boldsymbol{I}}$ is the unit dyadic, $\delta(\boldsymbol{r}-\boldsymbol{r}')$ the three-dimensional delta function, $k_B = 1.38\times10^{-23}$J/K the Boltzmann constant, $\Delta\omega$ the measured bandwidth around the center frequency ω ($\Delta\omega \ll \omega$ being assumed), $T(\boldsymbol{r})$ the temperature at point $\boldsymbol{r}$, and $\sigma(\boldsymbol{r})$ the corresponding conductivity. Note that in (1) the current density $\boldsymbol{J}$ is a phasor quantity (in A/m^2) and not a Fourier transform, usually denoted in the literature by $\boldsymbol{J}(\boldsymbol{r},\omega)$ [12].

The fluctuating random current densities $\boldsymbol{J}(\boldsymbol{r})$ are radiating in the presence of a lossy dielectric cylinder. Then, if the field induced at an external point due to an elementary current excitation $\bar{\boldsymbol{J}} = \bar{\boldsymbol{I}}\delta(\boldsymbol{r}-\boldsymbol{r}')$ inside the body is known, the total field can be computed by using the superposition principle. The response to this excitation is the dyadic Green's function $\bar{\boldsymbol{G}}(\boldsymbol{r},\boldsymbol{r}')$ of the infinite dielectric cylinder already treated in the literature [16], [17]. The dyadic Green's function $\bar{\boldsymbol{G}}(\boldsymbol{r},\boldsymbol{r}')$, when the source point $\boldsymbol{r}'$ is inside and the observation point $\boldsymbol{r}$ is outside the cylindrical body, can be written as follows:

$$\begin{aligned}\bar{\boldsymbol{G}}(\boldsymbol{r},\boldsymbol{r}') = \frac{j}{8\pi}\int_{-\infty}^{+\infty} dk \sum_{m=-\infty}^{+\infty}\frac{(-1)^m}{\alpha_0^2}\\ \cdot\Bigg(a_m(k)\boldsymbol{M}^{(3)}_{m,k}(\boldsymbol{r},k_0)\boldsymbol{M}^{(1)}_{-m,-k}(\boldsymbol{r}',k_1)\\ +\left(\frac{k_1}{k_0}\right)b_m(k)\boldsymbol{M}^{(3)}_{m,k}(\boldsymbol{r},k_0)\boldsymbol{N}^{(1)}_{-m,-k}(\boldsymbol{r}',k_1)\\ + b_m(k)\boldsymbol{N}^{(3)}_{m,k}(\boldsymbol{r},k_0)\boldsymbol{M}^{(1)}_{-m,-k}(\boldsymbol{r}',k_1)\\ + c_m(k)\boldsymbol{N}^{(3)}_{m,k}(\boldsymbol{r},k_0)\boldsymbol{N}^{(1)}_{-m,-k}(\boldsymbol{r}',k_1)\Bigg) \quad (2)\end{aligned}$$

where

$$\boldsymbol{M}^{(q)}_{m,k}(\boldsymbol{r},k_i) = \left(\frac{jm}{\rho}Z^{(q)}_m(\alpha_i\rho)\hat{\rho} - \frac{\partial Z^{(q)}_m(\alpha_i\rho)}{\partial\rho}\hat{\varphi}\right)e^{jm\varphi}e^{jkz} \quad (i=0,1) \quad (3)$$

$$\boldsymbol{N}^{(q)}_{m,k}(\boldsymbol{r},k_i) = \frac{1}{k_i}\nabla\times\boldsymbol{M}^{(q)}_{m,k}(\boldsymbol{r},k_i) \quad (4)$$

are the conventional cylindrical vector wave functions expressed in terms of the cylindrical coordinates ρ, φ, z shown in Fig. 1. The symbols $\hat{\rho}$, $\hat{\varphi}$, and $\hat{z}$ are to show the unit vectors along the ρ, φ, and z coordinates, respectively. The radial wave solutions $Z^{(q)}_m$ in (3) and (4) are

$$Z^{(q)}_m(x) = \begin{cases} J_m(x) & \text{(Bessel function) for } q=1\\ Y_m(x) & \text{(Neumann function) for } q=2\\ H^{(1)}_m(x) = J_m(x) + jY_m(x) & \text{(Hankel function) for } q=3. \end{cases} \quad (5)$$

Furthermore

$$k_0 = \omega\sqrt{\epsilon_0\mu_0} \qquad k_1 = k_0\sqrt{\epsilon_r + j\sigma/(\omega\epsilon_0)} \tag{6}$$

$$\alpha_0 = \left(k_0^2 - k^2\right)^{1/2} \qquad \alpha_1 = \left(k_1^2 - k^2\right)^{1/2} \tag{7}$$

with $\mathrm{Re}(\alpha_0)$, $\mathrm{Im}(\alpha_0) > 0$, so that the radiation conditions are satisfied when $\rho \to \infty$. The expansion coefficients $a_m(k)$, $b_m(k)$, and $c_m(k)$ are given in the Appendix.

In order to compute the random electric field $\boldsymbol{E}(\boldsymbol{r})$ out of the cylinder due to the random current density $\boldsymbol{J}(\boldsymbol{r})$, the superposition principle is employed, that is,

$$\boldsymbol{E}(\boldsymbol{r}) = j\omega\mu_0 \iiint_{V_0} d\boldsymbol{r}'\, \bar{\boldsymbol{G}}(\boldsymbol{r}, \boldsymbol{r}') \cdot \boldsymbol{J}(\boldsymbol{r}') \tag{8}$$

where V_0 is the infinite cylinder's volume. Then it is of interest to compute the average value $\langle \boldsymbol{E}(\boldsymbol{r}) \cdot \boldsymbol{E}^*(\boldsymbol{r}) \rangle$, which can be related to the stored energy density W (J/m^3) at an arbitrary point $\boldsymbol{r}$ outside the cylinder. Introducing (8) into the average value $\langle \boldsymbol{E} \cdot \boldsymbol{E}^* \rangle$ and rewriting $\bar{\boldsymbol{G}}(\boldsymbol{r}, \boldsymbol{r}')$ in compact form as

$$\bar{\boldsymbol{G}}(\boldsymbol{r}, \boldsymbol{r}') = \frac{j}{8\pi} \int_{-\infty}^{+\infty} dk \sum_{m=-\infty}^{+\infty} \frac{(-1)^m}{\alpha_0^2} e^{jm(\varphi - \varphi')} e^{jk(z-z')} \cdot \sum_{s=\rho,\varphi,z} \sum_{s'=\rho',\varphi',z'} g_{ss'}^{mk}(\rho, \rho') \hat{s}\hat{s}' \tag{9}$$

it is found that

$$\begin{aligned} &\langle \boldsymbol{E}(\boldsymbol{r}) \cdot \boldsymbol{E}^*(\boldsymbol{r}) \rangle \\ &= \left(\frac{\omega\mu_0}{8\pi}\right)^2 \iiint_{V_0} d\boldsymbol{r}' \iiint_{V_0} d\boldsymbol{r}'' \iint_{-\infty}^{+\infty} dk \int_{-\infty}^{+\infty} dk' \\ &\cdot \sum_{m=-\infty}^{+\infty} \sum_{m'=-\infty}^{+\infty} \frac{(-1)^{m+m'}}{\left(\alpha_0(k) a_0^*(k')\right)^2} \\ &\cdot \sum_{s_1=\rho,\varphi,z} \sum_{s_1'=\rho',\varphi',z'} \sum_{s_2=\rho,\varphi,z} \sum_{s_2'=\rho'',\varphi'',z''} \\ &\cdot \left\langle \left(g_{s_1 s_1'}^{mk}(\rho, \rho') \hat{s}_1 \hat{s}_1' \cdot \boldsymbol{J}(\boldsymbol{r}')\right) \cdot \left(g_{s_2 s_2'}^{*m'k'}(\rho, \rho'') \hat{s}_2 \hat{s}_2' \cdot \boldsymbol{J}^*(\boldsymbol{r}'')\right) \right\rangle \\ &\cdot e^{jm(\varphi - \varphi')} e^{-jm'(\varphi - \varphi'')} e^{jk(z-z')} e^{-jk'(z-z'')}. \end{aligned} \tag{10}$$

Writing the terms inside the brackets explicitly and using (1), the integration over the $\boldsymbol{r}''$ variable can be readily performed due to the $\delta(\boldsymbol{r}' - \boldsymbol{r}'')$ function. Then, taking into account the temperature distribution inside the cylinder:

$$T(\boldsymbol{r}) = T_0 + \begin{cases} \Delta T & \text{when } \boldsymbol{r} \in V_i \\ 0 & \text{when } \boldsymbol{r} \notin V_i \end{cases} \tag{11}$$

we can separate the integral with respect to $\boldsymbol{r}'$ (see (10)) into two parts. These two independent terms correspond to the contribution of the isothermal infinite cylinder and that of the inhomogeneity region. The former term is considerably simplified by employing the orthogonality relations

$$\int_0^{2\pi} d\varphi' e^{-j(m-m')\varphi'} = 2\pi\delta_{mm'} \tag{12}$$

$$\int_{-\infty}^{+\infty} dz' e^{-j(k-k')z'} = 2\pi\delta(k - k'). \tag{13}$$

Then

$$\begin{aligned} &\langle \boldsymbol{E}(\boldsymbol{r}) \cdot \boldsymbol{E}^*(\boldsymbol{r}) \rangle_0 \\ &= \frac{(\omega\mu_0)^2 k_B T_0 \sigma \Delta\omega}{4\pi} \int_{-\infty}^{+\infty} dk \sum_{m=-\infty}^{+\infty} \int_{\rho'=0}^{\alpha} \rho' d\rho' \frac{1}{|\alpha_0|^4} \\ &\cdot \sum_{s=\rho,\varphi,z} \sum_{s'=\rho',\varphi',z'} g_{ss'}^{mk}(\rho, \rho') g_{ss'}^{*mk}(\rho, \rho') \end{aligned} \tag{14}$$

where the subscript 0 in $\langle\,\rangle_0$ is to denote the homogeneous isothermal cylinder contribution. As will be shown in the next section, the integration over the ρ' variable in (14) can be performed analytically. Then a single integration over k and a single summation over m should be computed to obtain the numerical value of $\langle \boldsymbol{E} \cdot \boldsymbol{E}^* \rangle_0$.

In computing the contribution of the inhomogeneity region, the relations (12) and (13) cannot be used. Essentially, in addition to the integrations with respect to the k, k' variables and the summations over the m, m' integers, it is required to compute the integral over the inhomogeneity volume V_i. Considering the computer power limitations, it is clear that some form of approximation should be used. Taking into account the fact that in most cases the dimensions of the inhomogeneities are significantly smaller than the wavelength, and also that several V_i inhomogeneity regions could be used to model a larger inhomogeneity region, the integral over the volume V_i can be approximated as follows:

$$\iiint_{V_i} d\boldsymbol{r}' F(\boldsymbol{r}') \cong V_i F(\boldsymbol{r}_i) \tag{15}$$

where $\boldsymbol{r}_i = \rho_i(\cos\varphi_i \hat{x} + \sin\varphi_i \hat{y}) + z_i \hat{z}$ is the center of the inhomogeneity region and $F(\boldsymbol{r})$ is the integrand function. Then the inhomogeneity region contribution $\langle \boldsymbol{E} \cdot \boldsymbol{E}^* \rangle_i$ is found to be

$$\begin{aligned} \langle \boldsymbol{E}(\boldsymbol{r}) \cdot \boldsymbol{E}^*(\boldsymbol{r}) \rangle_i &= \left(\frac{\omega\mu_0}{8\pi}\right)^2 V_i \frac{4k_B \Delta T \sigma \Delta\omega}{\pi} \\ &\cdot \int_{-\infty}^{+\infty} dk \int_{-\infty}^{+\infty} dk' \sum_{m=-\infty}^{+\infty} \sum_{m'=-\infty}^{+\infty} \\ &\cdot \frac{1}{\left(\alpha_0(k) \alpha_0^*(k')\right)^2} \\ &\cdot \exp\left\{ j\left[(m-m')(\varphi - \varphi_i) + (k-k')(z - z_i)\right] \right\} \\ &\cdot \sum_{s=\rho,\varphi,z} \sum_{s'=\rho_i,\varphi_i,z_i} g_{ss'}^{mk}(\rho, \rho_i) g_{ss'}^{*m'k'}(\rho, \rho_i). \end{aligned} \tag{16}$$

Then the final result giving the total average value $\langle \boldsymbol{E}(\boldsymbol{r}) \cdot \boldsymbol{E}^*(\boldsymbol{r}) \rangle$ can be written as follows:

$$\langle \boldsymbol{E}(\boldsymbol{r}) \cdot \boldsymbol{E}^*(\boldsymbol{r}) \rangle = \langle \boldsymbol{E}(\boldsymbol{r}) \cdot \boldsymbol{E}^*(\boldsymbol{r}) \rangle_0 + \langle \boldsymbol{E}(\boldsymbol{r}) \cdot \boldsymbol{E}^*(\boldsymbol{r}) \rangle_i. \tag{17}$$

The electromagnetic energy stored per unit volume at an arbitrary point $\boldsymbol{r}$ outside the cylinder is computed from

$$W = W_0 + W_i \tag{18}$$

with

$$W_0 = \frac{\epsilon_0}{2}\langle \boldsymbol{E}(\boldsymbol{r})\cdot\boldsymbol{E}^*(\boldsymbol{r})\rangle_0 \tag{19}$$

$$W_i = \frac{\epsilon_0}{2}\langle \boldsymbol{E}(\boldsymbol{r})\cdot\boldsymbol{E}^*(\boldsymbol{r})\rangle_i \tag{20}$$

being the contributions of the $\langle \boldsymbol{E}\cdot\boldsymbol{E}^*\rangle_0$ and $\langle \boldsymbol{E}\cdot\boldsymbol{E}^*\rangle_i$ terms, respectively. Furthermore, in writing (19) and (20), the electric and magnetic energy densities are assumed to be equal (equipartition theorem).

It should be noted that in case of more than one inhomogeneity region, a summation over $\langle \boldsymbol{E}(\boldsymbol{r})\cdot\boldsymbol{E}^*(\boldsymbol{r})\rangle_i$ should appear in the right-hand side of (17).

III. Computation of the Integrals

First, the integration with respect to the ρ' variable in (14) is considered. Substituting the expressions for the $g_{ss'}^{mk}(\rho,\rho')$ tensor elements, as they are derived from the dyadic Green's function, and appropriately grouping the corresponding terms, standard integrals of Bessel (Hankel) function products are encountered and are easily computed using well-known formulas [18]. Then, in order to compute $\langle \boldsymbol{E}(\boldsymbol{r})\cdot\boldsymbol{E}^*(\boldsymbol{r})\rangle_0$, it is necessary to perform the integration over the k variable plus the summation over the m integer. A multisegment 16-point Gaussian quadrature numerical integration algorithm is employed. Then, even–odd symmetries with respect to the integration and summation variables are utilized to reduce the numerical computation cost. Convergence is checked automatically by increasing the number of integration segments and the truncation order for the summation until convergence is achieved. The $k \to +\infty$ upper bound is truncated at a sufficiently large value so that a good convergence is attained.

In computing the inhomogeneity region contribution $\langle \boldsymbol{E}\cdot\boldsymbol{E}^*\rangle_i$, similar numerical techniques are employed. In order to make the numerical work easier and faster, the separability of the integration variables k, k' and m, m' is utilized. That is,

$$\sum_m \sum_{m'} \int_{-\infty}^{+\infty} dk \int_{-\infty}^{+\infty} dk' \Phi(m,k)\Phi^*(m',k') = \left(\sum_m \int_{-\infty}^{+\infty} dk\, \Phi(m,k)\right)\left(\sum_{m'} \int_{-\infty}^{+\infty} dk' \Phi^*(m',k')\right) \tag{21}$$

where $\Phi(m,k)\Phi^*(m',k')$ is the integrand function appearing in (16).

IV. Computation of Black Body Radiation from an Infinite Cylinder (Radiative Transfer Theory)

In order to compare the results obtained by applying the electromagnetic wave theory for the $\langle E\cdot E^*\rangle_0$ homogeneous term, the thermal emission from a cylindrical body is computed using the classical radiative transfer concepts.

TABLE I
Numerical Results for the $U(\alpha/x_0)$ Integral Given in (26)

α/x_0	$U(\alpha/x_0)$
0.10	0.157
0.20	0.317
0.30	0.482
0.40	0.656
0.50	0.843
0.60	1.050
0.70	1 292
0 80	1.596
0.90	2.052
0.99	3.322
0.999	4.332

The observation point is taken to be on the x axis at $\boldsymbol{r} = x_0\hat{x}$ (see Fig. 1). According to the Rayleigh–Jeans theory [19], the spectral brightness ($\mathrm{Wm^{-2}Sr^{-1}s}$) of the emitting surface is given as

$$B_\omega = \frac{\omega^2 k_B T_0}{4\pi^3 c^2} \tag{22}$$

where $c = (\epsilon_0\mu_0)^{-1/2}$ is the free-space electromagnetic wave propagation velocity. The power passing through a unit area centered at $\boldsymbol{r} = x_0\hat{x}$ facing the cylinder is computed by summing the power densities originating from elementary areas dS on the cylinder surface. Then the total power density P_w ($\mathrm{W/m^2}$) at $\boldsymbol{r} = x_0\hat{x}$ can be written as follows:

$$P_w = \iint_{S_{\mathrm{obs}}} ds\, B_\omega\, d\Omega = \int_{-\infty}^{+\infty} dz' \int_{\varphi=-\varphi_0}^{\varphi_0} \alpha\, d\varphi'\, B_\omega R^{-2}. \tag{23}$$

Here S_{obs} is the observed cylinder surface,

$$d\Omega = 1(\mathrm{m^2})/R^2 = \left(x_0^2 + \alpha^2 - 2\alpha x_0 \cos\varphi' + z'^2\right)^{-1}$$

is the solid angle defined in Fig. 1, and

$$\varphi_0 = \cos^{-1}(\alpha/x_0) \tag{24}$$

defines the strip width on the cylinder surface illuminating the observation point. Substituting (22) into (23) and performing the integration over z', it is found that

$$P_\omega = \frac{\omega^2 k_B T_0}{2\pi^2 c^2} U(\alpha/x_0) \tag{25}$$

where

$$U(y) = \frac{y}{\sqrt{y^2+1}} \int_{\varphi'=0}^{\varphi_0} d\varphi' \left(1 - 2\frac{y}{y^2+1}\cos\varphi'\right)^{-1/2}. \tag{26}$$

The last integral can be computed numerically for any value of the ratio α/x_0. The energy stored per unit volume for an observation band width $\Delta\omega$ is computed from

$$W' = (P_\omega/c)\,\Delta\omega.$$

Then, using (25),

$$W' = \frac{\omega^2 k_B T_0 \Delta\omega}{2\pi^2 c^3} U(\alpha/x_0). \tag{27}$$

In Table I, results are given for the $U(\alpha/x_0)$ integral for several values of α/x_0. The integral in (26) is computed

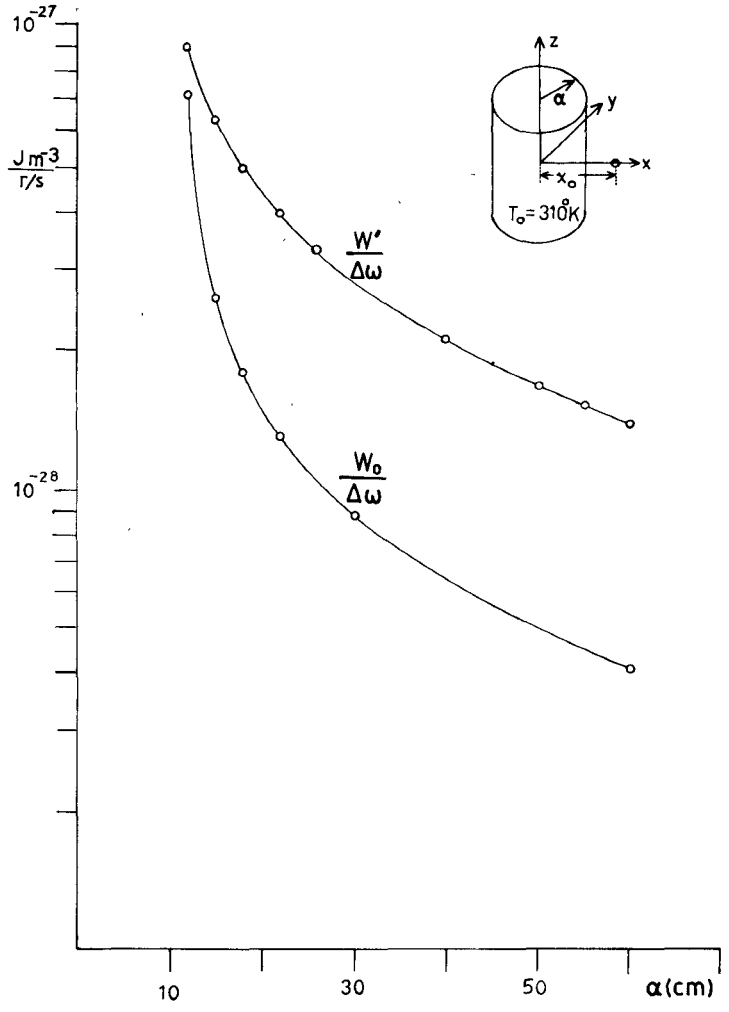

Fig. 2.

numerically by applying Simpson's rule. The emissivity factor ϵ can be defined for the isothermal cylinder by dividing (25) with (19):

$$\epsilon = \frac{W_0}{W'}. \tag{28}$$

In general, ϵ should be less than unity. It is shown in the next section that in general this condition is satisfied. However in case of strong reactive near fields, it is possible to have $\epsilon \geq 1$.

V. Numerical Results and Discussion

Numerical computations have been performed by applying the analytical results presented in Sections III and IV. First, the thermal radiation from a homogeneous isothermal cylinder is investigated. In Fig. 2, results are given for the stored energy densities per unit frequency bandwidth $W_0/\Delta\omega$ at several observations points for a cylinder of radius $\alpha = 10$ cm with $\epsilon_r = 50$, $\sigma = 1.3$ S/m, $T_0 = 310$ K, and center frequency 1.3 GHz. The values of ϵ_r and σ are complied from [17]. On the same figure, the corresponding computed black body energy densities are also presented. It is observed that in the vicinity of the cylinder surface, the stored energy density is approximately equal to the corresponding ideal black body value (i.e., $\epsilon \to 1$).

TABLE II
Computed Isothermal Stored Energy Densities $W_0/\Delta\omega$ (eq. (19)) and $W'/\Delta\omega$ Black Body Radiation (eq. (27)) at an Observation Point $r = x_0\hat{x} = 15$ cm $\hat{x}$ for a Cylinder of $\alpha = 10$ cm

$f = \omega/2\pi$ (MHz)	$W_0/\Delta\omega$ (Jm^{-3}/rs^{-1})	$W'/\Delta\omega$ (Jm^{-3}/rs^{-1})	σ (S/m)	ϵ_r
400	8.14×10^{-29}	6.05×10^{-29}	1.1	52
700	1.20×10^{-28}	1.85×10^{-28}	1.3	52
1300	2.61×10^{-28}	6.39×10^{-28}	1.3	50
3000	9.37×10^{-28}	3.4×10^{-27}	2.2	45

When the distance of the observation point from the cylinder surface gets larger ($x_0 > 2\alpha$), the observed emissivity factor drops rapidly (i.e., $W_0 \ll W'$). Furthermore, when $x_0 > 2\alpha$, the value of $\epsilon = W_0/W'$ is almost independent of the distance x_0 (see Fig. 2). We can take advantage of this fact to perform measurements of the thermal power very close to the human body surface. The strong energy density near the body surface is attributed to the reactive near-field components originating from the random current densities inside the body. Computations have also been performed for homogeneous isothermal cylinders at other frequencies. In Table II, $W_0/\Delta\omega$ and $W'/\Delta\omega$ values are given in the frequency range 400–3000 MHz for a

TABLE III
VARIATION OF THE W_i/W_0 RATIO WITH THE OBSERVATION POINT DISTANCE x_0 FROM THE BODY AXIS

$(x_0-\alpha)$ (cm)	(W_i/W_0)
2	1.122×10^{-3}
5	3.19×10^{-4}
8	1.35×10^{-4}
12	7.00×10^{-5}
16	4.60×10^{-5}
20	3.30×10^{-5}

The inhomogeneity is located on the x axis 1 cm below the body surface with $V_i=10$ cm^3 and ΔT (inhomogeneity region temperature increment) = 5 K. The observation point is sliding on the x axis. The center frequency is $\omega/2\pi=1.3$ GHz and the cylindrical body characteristics are $\alpha=10$ cm, $\epsilon_r=50$, and $\sigma=1.3$ S/m.

cylinder of radius $\alpha=10$ cm. The corresponding tissue dielectric permittivities ϵ_r and conductivities σ used in the computation [15] are also shown in the same table. The observation point is at a distance $x_0=15$ cm from the body axis. It is observed that the increase in the $W_0/\Delta\omega$ stored energy with the center frequency ω is less than that of the corresponding black body stored energy density $W'/\Delta\omega$. Furthermore, at 400 MHz center frequency numerical results shows that $\epsilon\cong1.3$. This exceptional result is explained by the fact that the stored reactive energy in the vicinity of the cylinder surface gets stronger at lower frequencies.

The presence of inhomogeneities has also been investigated numerically. To this end, the ratios W_i/W_0 of the inhomogeneity to the isothermal cylinder energy density have been computed for several values of inhomogeneity volumes V_i and temperature differences ΔT. Comparison of W_i/W_0 values for different inhomogeneity positions for a given observation point provides information for the detectability of high-temperature regions within the body. In Table III, results are given for the ratio W_i/W_0 at several observation points outside the cylinder for an inhomogeneity of volume $V_i=10$ cm^3 located 1 cm below the body surface. The temperature difference is $\Delta T=5$ K and the center frequency $f=\omega/2\pi=1.3$ GHz. The cylinder radius is again $\alpha=10$ cm with $\epsilon_r=50$ and $\sigma=1.3$ S/m. The inhomogeneity center and the observation points are taken to be on the x axis. It is shown that when the observation point is far from the body surface (not more than two or three times the inhomogeneity depth), the ratio W_i/W_0 is very small. Significant values of W_i/W_0 are observed when the observation point is very close to the body surface. This is explained by considering the large amount of thermal power emission from the whole cylindrical body in comparison to the small volume inhomogeneity thermal radiation power. Only for observation points very close to the inhomogeneity region could significant values of W_i/W_0 be obtained. Nevertheless, particular computations advocate the use of microwave radiometers to estimate temperature distributions within superficial tissues. In principle, it is possible to argue that,

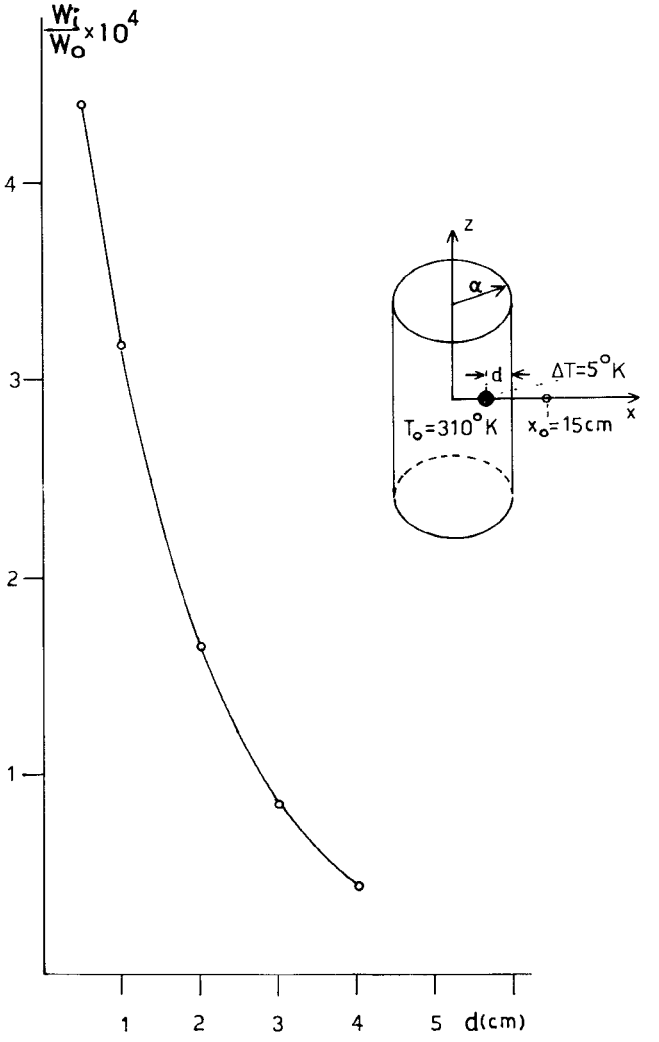

Fig. 3.

if the reactive near-field energy densities are measured, some information could be obtained for the temperature levels inside superficial tissues.

In Fig. 3, the variation of W_i/W_0 with respect to the depth d of the inhomogeneity center from the body surface for $\Delta T=5$ K, $V_i=10$ cm^3, $x_0=15$ cm, $\alpha=10$ cm, $f=1.3$ GHz center frequency, $\epsilon_r=50$, and $\sigma=1.3$ S/m. It is observed that the computed W_i/W_0 values diminish rapidly as the inhomogeneity depth gets large. Indeed, when $d>2$ cm (see Fig. 3), the variation of W_i/W_0 decreases exponentially with the inhomogeneity depth. When $d<2$ cm, there is a very steep increase in the external observed thermal emission radiation energy density.

Finally, the resolution capability in locating inhomogeneities within the human body is investigated by scanning the observation point parallel to cylinder surface. Again, the center frequency is $f=\omega/2\pi=1.3$ GHz. The observation point is moving on a cylindrical surface $\rho=\rho_0$ (constant) (see Fig. 1) while the inhomogeneity center is on the x axis 1 cm below the body surface. The cylindrical body radius is $\alpha=10$ cm and again $\epsilon_r=50$ and $\sigma=1.3$ S/m. The inhomogeneity volume is $V_i=10$ cm^3 and $\Delta T=10$ K. The maximum total energy density $W_M=(W_0+W_i)_M$ is observed when the observation point is also on

TABLE IV
VARIATION OF $(1-W(\varphi,z)/W_M)\times 10^3$ WHEN THE OBSERVATION POINT IS SCANNING ON A $\rho=\rho_0$ (CONSTANT) SURFACE

		$(1-W(\varphi,z)/W_M)\times 10^3$	
z (cm)	$\alpha\varphi$ (cm)	$\rho_0=15$ cm	$\rho_0=12$ cm
0	0	0	0
2	0	0.15	0.53
4	0	0.37	—
0	2	0.07	0.66
0	4	0.21	—

The inhomogeneity volume $V_i=10$ cm^3 and $\Delta T=10$ K. The homogeneous cylinder radius $\alpha=10$ cm, $\epsilon_r=50$, and $\sigma=1.3$ S/m. The center frequency $f=\omega/2\pi=1.3$ GHz and the inhomogeneity center depth is 1 cm below the body surface.

the x axis (i.e., $z=0$, $\varphi=0$). In Table IV, the variation of $(1-W(\varphi,z)/W_M)\times 10^3$ is given for $\rho_0=15$ cm and $\rho_0=12$ cm, where $W(\varphi,z)$ is the energy density observed at $\boldsymbol{r}=\rho_0(\cos\varphi\hat{x}+\sin\varphi\hat{y}+z\hat{z})$ (cm) (see Fig. 1).

It is shown that there is a 0.1–0.5‰ order variation in $W(\varphi,z)$ for 2–4 cm lateral displacements from the nearest point to the inhomogeneity region, where maximum energy density is observed (i.e., $W=W_M$). The rather small variation observed in the percentage variation of $W(\varphi,z)$ is attributed to the fact that the global thermal emission from surrounding tissues is very strong in comparison with the emission from the inhomogeneity volume thermal sources.

Therefore, the background radiation from the tissues can mask the emission from a small inhomogeneity region. It seems that this is the main problem in microwave radiometry noninvasive thermometry systems rather than the limited transparency of tissues. A well-designed antenna could enhance the emission from specific points within the body. Also, extensive experimental data are needed to estimate the limitation of microwave radiometry systems as non-invasive thermometers.

VI. CONCLUSIONS

The microwave thermal emission from a cylindrical human body model has been analyzed by applying electromagnetic theory techniques. The radiative transfer theory is also employed to compare the results obtained by using the electromagnetic approach for an isothermal homogeneous cylinder. Dyadic Green's function techniques proved to be suitable in computing the stored energy density of the thermal microwave radiation. The feasibility of using microwave radiometry in measuring the in-depth temperature distributions inside a human body is investigated. It is shown that in principle it is possible to estimate average properties of temperature distributions within the body by measuring the emitted microwave power in the near-field region of thermal sources. There is a strong energy accumulation in the vicinity of superficial tissues. Especially in hyperthermia applications, where rather large temperature gradients (ΔT) are encountered, microwave radiometry can provide an effective noninvasive thermometry technique.

It is shown that the use of low microwave frequencies ($\sim$1 GHz) could provide a measurement depth of the order of 1–2 cm. However, the corresponding spatial resolution capability is rather low, of the order of 3–4 cm. In this paper, only the stored energy per unit volume of the thermal power has been investigated. In practice, an antenna should be used to collect and measure the thermal radiation intensity. The analysis of the received power in an aperture antenna and the imaging properties of an experimental 1.3-GHz radiometer with a dielectric loaded waveguide antenna will be examined elsewhere. The most suitable receiving antenna seems to be a dielectric loaded open waveguide. Furthermore, the moderate directivity properties of the loaded open waveguide would enhance the received power from thermal inhomogeneities within the body and suppress the power received from the surrounding isothermal tissues.

APPENDIX
DEFINITION OF THE $a_m(k)$, $b_m(k)$, AND $c_m(k)$ TERMS IN (2)

$$a_m(k)=\frac{H_m^{(1)}(x_1)}{H_m^{(1)}(x_0)}\frac{\epsilon_r}{\Delta_m}\left[\left(\frac{1}{\alpha_1}\frac{J_m'(x_1)}{J_m(x_1)}\right)^2+\frac{1}{\alpha_0}\frac{H_m'^{(1)}(x_0)}{H_m^{(1)}(x_0)}\frac{1}{\alpha_1}\frac{H_m'^{(1)}(x_1)}{H_m^{(1)}(x_1)}-\frac{1}{\alpha_0}\frac{H_m'(x_0)}{H_m^{(1)}(x_0)}\frac{1}{\alpha_1}\frac{J_m'(x_1)}{J_m(x_1)}-\frac{1}{\alpha_1}\frac{H_m'^{(1)}(x_1)}{H_m^{(1)}(x_1)}\frac{1}{\alpha_1}\frac{J_m'(x_1)}{J_m(x_1)}\right]$$

$$b_m(k)=-\frac{2j}{\pi}\frac{1}{H_m^{(1)}(x_0)}\frac{(\dot{\epsilon}_r-1)mk}{J_m(x_1)}\frac{1}{\Delta_m}\frac{k_0}{\alpha_1^4x_0^2}$$

$$c_m(k)=\frac{H_m^{(1)}(x_1)}{H_m^{(1)}(x_0)}\frac{1}{\Delta_m}\left[\dot{\epsilon}_r\left(\frac{J_m'(x_1)}{\alpha_1J_m(x_1)}\right)^2-\frac{1}{\alpha_0}\frac{H_m'^{(1)}(x_0)}{H_m^{(1)}(x_0)}\frac{1}{\alpha_1}\frac{J_m'(x_1)}{J_m(x_1)}+\frac{1}{\alpha_0}\frac{H_m'^{(1)}(x_0)}{H_m^{(1)}(x_0)}\frac{1}{\alpha_1}\frac{H_m'^{(1)}(x_1)}{H_m^{(1)}(x_1)}-\dot{\epsilon}_r\frac{1}{\alpha_1}\frac{J_m'(x_1)}{J_m(x_1)}\frac{1}{\alpha_1}\frac{H_m'^{(1)}(x_1)}{H_m^{(1)}(x_1)}\right]$$

$$\Delta_m=\dot{\epsilon}_r\left(\frac{1}{\alpha_1}\frac{J_m'(x_1)}{J_m(x_1)}\right)^2+\left(\frac{1}{\alpha_0}\frac{H_m'^{(1)}(x_0)}{H_m^{(1)}(x_0)}\right)^2-(\dot{\epsilon}_r+1)\frac{1}{\alpha_0}\frac{H_m'^{(1)}(x_0)}{H_m^{(1)}(x_0)}\frac{1}{\alpha_1}\frac{J_m'(x_1)}{J_m(x_1)}-\frac{k_0^2m^2k^2(\dot{\epsilon}_r-1)^2}{\alpha_1^4\alpha_0^4\alpha^2}$$

$$x_1=\alpha_1\alpha \qquad x_0=\alpha_1\alpha \qquad \dot{\epsilon}_r=\epsilon_r+j\frac{\sigma}{\omega\epsilon_0}.$$

REFERENCES

[1] A. H. Barret and P. C. Myers, "A method of detecting subsurface thermal patterns," *Biol. Radiol.*, no. 6, pp. 45–46, 1975.

[2] K. L. Carr, A. M. El Mahdi, and J. Schaffer, "Dual mode microwave system to enhance early detection of cancer," *IEEE Trans. Microwave Theory Tech.*, vol. MTT-29, pp. 256–260, 1981.

[3] T. C. Cetas, "Will thermometric tomography become practical for hyperthermia monitoring?," *Cancer Res.*, vol. 44, pp. 48055–48085, 1984.

[4] J. Edrich, "Centimeter—and millimeter—wave thermography, A survey on tumor detection," *J. Microwave Power*, vol. 14, pp. 95–104, 1979.

[5] P. C. Myers, N. L. Sadowsky, and A. H. Barret, "Microwave thermography: Principles, methods and clinical applications," *J. Microwave Power*, vol. 14, pp. 105–114, 1979.

[6] J. Edrich and P. C. Hardee, "Thermography at millimeter wavelengths," *Proc. IEEE*, vol. 62, pp. 1391–1392, 1974.

[7] M. Chive, M. Plancot, G. Giaux, and B. Prevost, "Microwave hyperthermia controlled by microwave radiometry: Technical aspects and first clinical results," *J. Microwave Power*, vol. 19, pp. 233–241, 1984.

[8] C. Pichot, L. Jofre, G. Peronnet, and J. C. Bolomey, "Active microwave imaging of inhomogeneous bodies," *IEEE Trans. Antennas Propagat.*, vol. AP-33, pp. 416–425, 1985.

[9] J. W. Strohbehn and E. B. Douple, "Hyperthermia and cancer therapy: A review of biomedical engineering contributions and challenges," *IEEE Trans. Biomed. Eng.*, vol. BME-31, pp. 779–787, 1984.

[10] F. T. Ulaby, R. K. Moore, and A. K. Fung, *Microwave Remote Sensing, Active and Passive*, vol. 1. Reading, MA: Addison-Wesley, 1981.

[11] S. Chandrasekhar, *Radiative Transfer*. New York: Dover, 1960.

[12] L. Tsang, J. A. Kong, and R. T. Shin, *Theory of Microwave Remote Sensing*. New York: Wiley, 1985.

[13] S. M. Rytov, "Theory of electric fluctuations and thermal radiation," AD 226765, Defense Documentation Center, Arlington, VA, 1959.

[14] G. W. Kattawar and M. Eisner, "Radiation from a homogeneous isothermal sphere," *Appl. Opt.*, vol. 9, pp. 2685–2690, 1970.

[15] H. P. Schwan and K. R. Foster, "RF-field interactions with biological systems electrical properties and biophysical mechanisms," *Proc. IEEE*, vol. 68, pp. 104–113, 1980.

[16] D. A. Hill and J. R. Wait, *Applied Physics*, vol. 6. New York: Springer Verlag, 1978, pp. 391–398.

[17] N. K. Uzunoglu, "Scattering from inhomogeneities inside a fiber waveguide," *J. Opt. Soc. Amer.*, vol. 71, pp. 259–273, 1981.

[18] M. Abramowitz and I. Stegun, *Handbook of Mathematical Functions*. New York: Dover, 1965, ch. 11.

[19] F. T. Ulaby, R. K. Moore, and A. K. Fung, *Microwave Remote Sensing, Active and Passive*, vol. 1. Reading, MA: Addison-Wesley, 1981, ch. 4.

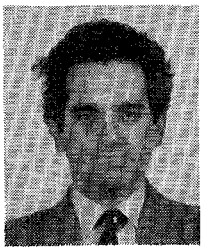

Nikolaos K. Uzunoglu (M'82) received the B.Sc. degree in electronics engineering from the Istanbul Technical University, Turkey, in 1973. He obtained the M.Sc. and Ph.D. degrees from the University of Essex, England, in 1974 and 1976, respectively.

He worked for the Hellenic Navy Research and Technology Development Office from 1977 to 1984. During this period, he also worked on a part-time basis at the National Technical University on electromagnetic theory. In 1984, he was elected Associate Professor at the National Technical University of Athens, the position that he holds presently. His research interests are microwave applications, fiber optics, and electromagnetic theory.

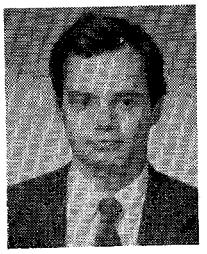

P. G. Cottis was born in Salonica, Greece, in 1956. He received the Diploma degree in electrical engineering from the National Technical University of Athens (NTUA) in 1979, the M.Sc. degree in communication engineering from the University of Manchester in 1980, and the Doctor's degree in electrical engineering from NTUA in 1984.

Since 1981, he has been working as a Research Associate in the Department of Electrical Engineering at NTUA. His main research interest is electromagnetic fields, with emphasis on scattering and propagation at millimeter and optical wavelengths.

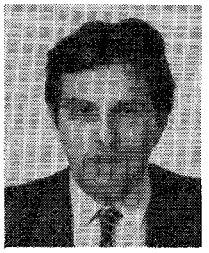

Petros S. Papakonstantinou was born in Athens, Greece, on January 8, 1959. He graduated from London University, where he received the B.Sc. degree in physics and the M.Sc. degree in electrical engineering. Presently he is working for the Ph.D. degree in the Department of Electrical Engineering at the National Technical University of Athens on the medical applications of microwave radiometry.